Auger effect in the presence of strong x-ray pulses

Ji-Cai Liu,[1,2] Yu-Ping Sun,[1,2,*] Chuan-Kui Wang,[1,2] Hans Ågren,[2] and Faris Gel'mukhanov[2]
[1]*College of Physics and Electronics, Shandong Normal University, 250014 Jinan, People's Republic of China*
[2]*Theoretical Chemistry, School of Biotechnology, Royal Institute of Technology, S-106 91 Stockholm, Sweden*
(Received 15 December 2009; published 19 April 2010)

We study the role of propagation of strong x-ray free-electron laser pulses on the Auger effect. When the system is exposed to a strong x-ray pulse the stimulated emission starts to compete with the Auger decay. As an illustration we present numerical results for Ar gas with the frequency of the incident x-ray pulse tuned in the $2p_{3/2}$-$4s$ resonance. It is shown that the pulse propagation is accompanied by two channels of amplified spontaneous emission, $4s$-$2p_{3/2}$ and $3s$-$2p_{3/2}$, which reshape the pulse when the system is inverted. The population inversion is quenched for longer propagation distances where lasing without inversion enhances the Stokes component. The results of simulations show that the propagation of the strong x-ray pulses affect intensively the Auger branching ratio.

DOI: 10.1103/PhysRevA.81.043412 PACS number(s): 32.80.Hd, 32.80.Aa, 42.55.Vc, 42.50.Hz

I. INTRODUCTION

Short and intense x-ray pulses from x-ray free-electron lasers (XFEL) [1,2] will provide the possibility to overcome the limitations of present-day synchrotron radiation light sources like low intensity and long pulse duration. While several examples of the strong x-ray field effects have been studied recently [3–6], the role of the strong x-ray pulse propagation through a resonant medium has not been studied yet. In our previous articles [7–9] we paid attention to the reshaping of x-ray pulses during propagation caused by the stimulated resonant Raman scattering (SRRS), which starts from amplified spontaneous emission (ASE) followed later on by lasing without inversion (LWI). The main goal of the present article is to investigate the role of propagation of strong resonant x-ray pulses on relative Auger yield. This problem is important in x-ray spectroscopy because the Auger process is the major effect which determines the dynamics of the atoms and molecules in core-excited states [10].

The Auger process is undesirable in the sense of radiation damage of the sample in a single XFEL pulse. The radiation damage is mainly introduced by the ionization followed by Coulomb explosion (see [11] and references therein). The ionization of light elements occurs mainly because of the Auger decay in the case of resonant x-ray scattering. Thus the key question becomes how to suppress the Auger effect. Auger process can be affected by a strong x-ray field due to two reasons. The first one is the high-field multi-electron excitation or ionization, which directly changes the Auger rate Γ due to reorganization of the electron structure. In this study we focus on the second mechanism where the strong x-ray field does not change the Auger rate Γ itself, but it changes the relative Auger rate or Auger branching ratio. When the x-ray field is strong enough, the population of the core-excited state is followed by stimulated emission. Therefore, there will be competition between the Auger decay and the stimulated emission inside the pulse. For example, the Auger process has no time to occur if the stimulated emission is faster than the Auger decay. Recently, Rohringer and Santra [4] studied how the stimulated emission affects the Auger yield without taking into account the propagation effects, assuming an optically thin medium. They found strong changes of the Auger yield for a 2π x-ray pulse. However, the role of pulse reshaping during propagation can be significant in a real experiment performed with samples of finite size.

We study here the propagation of the strong x-ray pulse through the resonant medium of atomic Ar and show that the reshaping of the x-ray pulse strongly affects the relative Auger rate. The carrier frequency of the input pulse is tuned in resonance with the $2p_{3/2}$-$4s$ transition. The pulse reshaping starts from two ASE channels, $4s$-$2p_{3/2}$ and $3s$-$2p_{3/2}$ with the transition energies $\hbar\omega_{10} = 244.3$ eV [12] and $\hbar\omega_{12} = 219.28$ eV [13]. Subsequently, the lasing will occur without population inversion. Our theoretical model is based on strict numerical solutions of the coupled density matrix and Maxwell's equations for three-level atoms.

The paper is organized as follows. We start with an analysis of the Auger yield and the relative Auger yield (Sec. II). Section III is devoted to discussions of the results obtained. Our findings are summarized in Sec. IV.

II. FORMULATION OF AUGER YIELD AND RELATIVE AUGER YIELD

To exemplify the theory we study the interaction of x rays with Ar atoms near the L_{III} absorption threshold. The strong x-ray field couples the core-excited state ($|1\rangle = |2p_{3/2}^{-1}4s\rangle$) with the ground ($|0\rangle$) and the Stokes ($|2\rangle = |3s^{-1}4s\rangle$) states (Fig. 1).

In fact, the studied system is not a three-level system because of the nonzero angular momentum of the core hole. The degeneracy of the $2p_{3/2}$ core level deserves a special comment. This core level has four degenerated sublevels: $|3/2m\rangle = \sqrt{1/2 + m/3}Y_{1m-1/2}\alpha + \sqrt{1/2 - m/3}Y_{1m+1/2}\beta$, $m = \pm 1/2, \pm 3/2$. Here α and β are the spin wave functions with up and down spin orientations, respectively. We study here the stimulated scattering of the x-ray photon where the polarization vector $\mathbf{e}$ does not change during pulse propagation. Due to the spherical symmetry of atoms, the axis of quantization z can be chosen arbitrarily. It is convenient

*yuping@theochem.kth.se

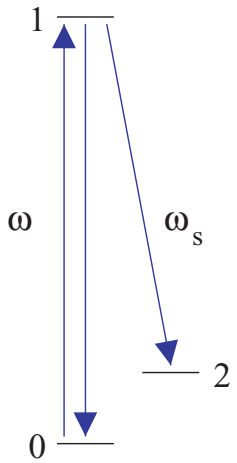

FIG. 1. (Color online) Scheme of resonant (0-1) and Stokes (1-2) transitions in argon atom. $|1\rangle = |2p_{3/2}^{-1}4s\rangle$, $|2\rangle = |3s^{-1}4s\rangle$.

to orient z along **e**. In this case we have two independent scattering channels $2p_{3/2,1/2} \to 4s\alpha$, $ns\alpha \to 2p_{3/2,1/2}$ and $2p_{3/2,-1/2} \to 4s\beta$, $ns\beta \to 2p_{3/2,-1/2}$. This means that the studied problem is reduced to pulse propagation through a three-level system. (Fig. 1, for more details see Ref. [9]).

The transition dipole moments $d_{10} = 0.14$ a.u. and $d_{21} = 0.32$ a.u. [8] are obtained using the experimental data [14,15] and *ab initio* simulations [16]. The carrier frequency ω of the incident x-ray pulse is tuned in resonance with the transition $0 \to 1$ ($\omega = \omega_{10}$).

Let us first write down the equations for the population of the core-excited state $|1\rangle$ and for the total population of the intact atoms, which we need to analyze the Auger process

$$\left(\frac{\partial}{\partial t} + \Gamma\right)\rho_{11} = W,$$
$$\frac{\partial}{\partial t}(\rho_{00} + \rho_{11} + \rho_{22}) = -\Gamma\rho_{11} - \Gamma_f\rho_{22}. \tag{1}$$

SI units are used. Mainly the Auger decay forms the full width at half maximum (FWHM) of the x-ray absorption lines of light atoms like Ar, hence the small spontaneous decay rates are neglected here. $\hbar\Gamma = 0.12$ eV [12,17–19] and $\hbar\Gamma_f = 0.076$ eV [20] are the Auger broadenings of the core-excited state $|1\rangle$ and the final state $|2\rangle$, respectively. To make equations more compact we use for brevity the shortened notations like $\rho_{ii} \equiv \rho_{ii}(t,y)$.

The rate of population of the core-excited state by the x-ray field is given by the expectation value of the commutator $W = \imath[V,\rho]_{11}$ of the density matrix with the operator of dipole interaction V between the atoms and the x-ray field $E(t,y)$. In fact, W is positive only when the field is weak. We study the case of strong XFEL pulse where the absorption ($W > 0$) is followed by stimulated emission ($W < 0$), and so on. The manifestation of this sign-changing behavior of the field work W is the Rabi oscillations of the population. The probability of radiative population or depopulation of the core-excited state

$$W = 2\,\mathrm{Im}\sum_{n=0,2} V_{1n}\rho_{n1}, \quad V_{nm} = -\frac{1}{\hbar}E(t,y)d_{nm}e^{\imath\omega_{nm}t}, \tag{2}$$

depends on the strength of the electromagnetic field $E(t,y)$, which changes during pulse propagation along the y axis according to Maxwell's equations

$$\frac{\partial E}{\partial y} + \mu_0\frac{\partial H}{\partial t} = 0, \quad \frac{\partial H}{\partial y} + \epsilon_0\frac{\partial E}{\partial t} = -\frac{\partial P}{\partial t}. \tag{3}$$

Here d_{nm} and $\hbar\omega_{nm} = E_n - E_m$ are the dipole moment and resonant energy of the $n-m$ transition, respectively. The pulse propagates along the y axis ($y \geqslant 0$) with the entry in the medium at $y = 0$. The population of the core-excited state generates new fields related to the decay transitions $|1\rangle \to |0\rangle$ and $|1\rangle \to |2\rangle$. Maxwell's equations take into account all fields $E(t,y)$, including the incident x-ray field and the new fields generated during pulse propagation, through the light-induced polarization $P(t,y) = N\,\mathrm{Tr}(d\hat{\rho})$. Here N is the concentration of the atoms. $E \equiv E_z(t,y)$, $H \equiv H_x(t,y)$. The density matrix $\hat{\rho} \equiv \hat{\rho}(t,y)$ is normalized to 1 for $t = -\infty$ when only the ground state is populated, $\rho_{00}(-\infty) = 1$, $\rho_{11}(-\infty) = \rho_{22}(-\infty) = 0$. It is worthwhile to mention that the total population of the neutral Ar atoms $\rho = \rho_{00} + \rho_{11} + \rho_{22}$ decreases due to the Auger decay when the system is shined by the x rays. Only the total population of the neutral atoms and the ions created in the course of Auger decay should be constant: $\rho + \rho_{\mathrm{ion}} = 1$.

The quantitative characteristic of the Auger process is the total number of the Auger transitions $\rho_{\mathrm{Aug}}(y)$, which is nothing other than $\rho_{\mathrm{ion}}(\infty,y) = 1 - \rho(\infty,y)$, where $\rho(\infty,y) = \rho_{00}(\infty,y) + \rho_{11}(\infty,y) + \rho_{22}(\infty,y) = \rho_{00}(\infty,y)$ is the number of the neutral (intact) atoms after the pulse ($t = \infty$). The number of intact atoms decreases according to the second equation in Eq. (1). The integration of this equation gives the number of Auger decay events [4]

$$\rho_{\mathrm{Aug}}(y) = \rho_{\mathrm{Aug}}^{(1)}(y) + \rho_{\mathrm{Aug}}^{(2)}(y) = 1 - \rho(\infty,y)$$
$$= \Gamma\int_{-\infty}^{\infty}\rho_{11}(t,y)dt + \Gamma_f\int_{-\infty}^{\infty}\rho_{22}(t,y)dt. \tag{4}$$

One can see that the total Auger yield is caused by the Auger decay of the core-excited state $|1\rangle = |2p_{3/2}^{-1}4s\rangle$ and of the final state $|2\rangle = |3s^{-1}4s\rangle$. The Auger yield defined by Eq. (4) corresponds to the Auger yield per initial atom $\rho_{\mathrm{Aug}} = R_{\mathrm{Aug}}/N$, where R_{Aug} is the Auger yield related to the initial concentration of atoms N. Thus, to get the Auger yield per volume (R_{Aug}), we have to multiply ρ_{Aug} by N. In the following we will focus our attention only on the partial Auger yield caused by the decay of the core-excited state

$$\rho_{\mathrm{Aug}}(y) \to \rho_{\mathrm{Aug}}^{(1)}(y) = \Gamma\int_{-\infty}^{\infty}\rho_{11}(t,y)dt. \tag{5}$$

This expression has to be used for the studied problem rather carefully. Indeed, one can get "strong suppression" of the Auger yield when the light intensity is small. But this suppression is trivial because this happens only due to the small number of core-excited atoms. As already mentioned in the Introduction, we need to consider the relative Auger yield, which refers directly to the competition between Auger and radiative (stimulated emission) decay channels.

To obtain the relative Auger yield it is instructive to look at the so-called field work W (2). Figure 2 shows the sign-changing modulation of $W = W(t,y)$ when the field is strong.

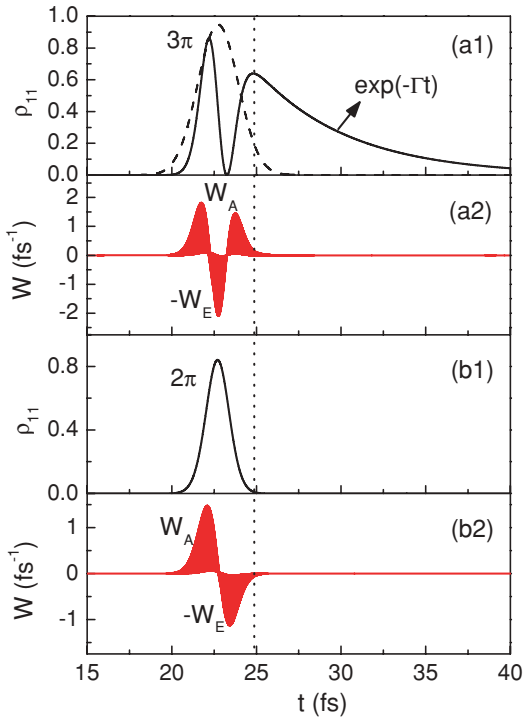

FIG. 2. (Color online) The field work $W(t,y)$ and the population of the core-excited state ρ_{11}; $\tau = 2$ fs, $y = 0.0001$ μm, and $\omega = \omega_{10}$. The envelope of the input pulse $\mathcal{E}(t,0)$ is shown (in arb. units) by the dashed line. (a) $\theta = 3\pi$, $\mathcal{E}_0 = 2.91 \times 10^9$ V/cm, $I_0 = c\epsilon_0\mathcal{E}_0^2/2 = 1.12 \times 10^{16}$ W/cm^2. (b) $\theta = 2\pi$, $\mathcal{E}_0 = 1.94 \times 10^9$ V/cm, $I_0 = 4.98 \times 10^{15}$ W/cm^2.

The main reason for this modulation is the Rabi oscillation, which can be seen already for the two-level system ($\Gamma = 0$, $\omega = \omega_{10}$, $d_{12} = 0$)

$$W(t,y) = \frac{G(t,y)}{2}\sin\theta(t,y), \quad \rho_{11}(t,y) = \sin^2\frac{\theta(t,y)}{2}, \tag{6}$$

where

$$\theta(t,y) = \int_{-\infty}^{t} G(t_1,y)dt_1, \tag{7}$$

is the pulse area at the instant t and $G(t,y) = d_{10}\mathcal{E}(t,y)/\hbar$ is the instantaneous Rabi frequency, $\mathcal{E}(t,y)$ is the envelope of the field. At the beginning of pulse propagation, $y \simeq 0$, the third level 2 does not play any role, and the only difference between the strict numerical solution for the studied three-level model (Fig. 2) and the Rabi solution (6) is Γ, which makes $W(t,0)$ asymmetrical. Figure 2 displays a general strong field effect, namely, the absorption of the laser field is followed by the stimulated emission. The number of oscillations of $W(t,y)$ depends on the pulse area and on the number of nodes of the envelope $\mathcal{E}(t,y)$ as seen from Eq. (6). Taking into account this fact, it is instructive to divide W into positive ($W_A > 0$) and negative ($-W_E < 0$) parts

$$W = W_A - W_E, \tag{8}$$

which correspond to the population (absorption) and depopulation (stimulated emission) of the core-excited state. The rates W_A and $-W_E$ will be calculated numerically in the following as the positive and negative parts of the field work W using Eq. (2). Equation (8) allows us to rewrite the rate equation for ρ_{11} in a physically clear form

$$\frac{\partial\rho_{11}}{\partial t} = -(\Gamma\rho_{11} + W_E) + W_A. \tag{9}$$

The right-hand side of this equation says that the core-excited state, populated with rate W_A, is depopulated due to the Auger decay ($\Gamma\rho_{11}$) and the stimulated emission W_E. This allows us to introduce the instantaneous relative Auger yield of the Auger decay $w(t,y) = \Gamma\rho_{11}/(\Gamma\rho_{11} + W_E)$. Instead, we use, in the following, the integral relative Auger yield as the ratio of the Auger rate to the total rate of depopulation of the core-excited state at the point y

$$w(y) = \frac{\rho_{\rm Aug}(y)}{\rho_{\rm Aug}(y) + \rho_E(y)}, \quad \rho_E(y) = \int_{-\infty}^{\infty} W_E(t,y)dt, \tag{10}$$

which is consistent with the strict balance equation (9)

$$\int_{-\infty}^{\infty} W_A(t,y)dt = \int_{-\infty}^{\infty}[\Gamma\rho_{11}(t,y) + W_E(t,y)]dt. \tag{11}$$

This particle conservation law expresses that the total number of core excitations is equal to the total number of decay events, namely, the number of Auger transitions (5) plus the number of stimulated emission transitions $\rho_E(y)$ (10).

It can be useful also to know the total number of the Auger $[N_{\rm Aug}(L)]$ and stimulated emission $[N_E(L)]$ decay transitions collected from the whole sample of length L and the related integral branching ratio

$$q(L) = \frac{N_{\rm Aug}(L)}{N_{\rm Aug}(L) + N_E(L)}, \qquad N_j(y) = \int_0^L \rho_j(y)dy, \quad j = {\rm Aug}, E. \tag{12}$$

The main reason for the suppression of the Auger yield is the stimulated emission which depopulates the core-excited state faster than the Auger decay when the x-ray field is high enough. The quantitative characteristic of this competition is the relative Auger yield $w(y)$ (10) and $q(L)$ (12). The experimental measurement of $w(y)$ and $q(L)$ is more difficult than the measurement of the Auger yield $\rho_{\rm Aug}$ because it requires femtosecond temporal resolution to obtain W_E (see Figs. 2 and 3). Let us show the principal possibility of doing this in the region $y < y_c$ where the population of the final state is negligibly small $\rho_{22} \approx 0$ [Fig. 4(b)]. First we need to measure the concentration of the ions $N_{\rm ion}$ at the instant t to obtain $\rho_{\rm ion} \equiv N_{\rm ion}/N$. Now we are in the stage to get the population of the core-excited state $\rho_{11} = \dot\rho_{\rm ion}/\Gamma$ and the field work $W = \ddot\rho_{\rm ion}/\Gamma + \dot\rho_{\rm ion}$ using Eq. (1) and $\rho + \rho_{\rm ion} = 1$. When the time evolution of W is established we can define the rate of the stimulated emission W_E as the negative part of the field work (see Figs. 2 and 3) as it was discussed already.

The numerical simulations are performed for the input pulse $E_0(t,y) = \mathcal{E}(t,y)\cos(\omega t - ky)$ with a Gaussian shape

$$\mathcal{E}(t,y) = \mathcal{E}_0 \exp\left[-2\ln 2\left(\frac{t - y/c - t_0}{\tau}\right)^2\right]. \tag{13}$$

Here τ is the FWHM of the intensity profile of the pulse $k = \omega/c$. The Bloch and Maxwell's equations are solved by use of an iterative predictor-corrector finite-difference time-domain

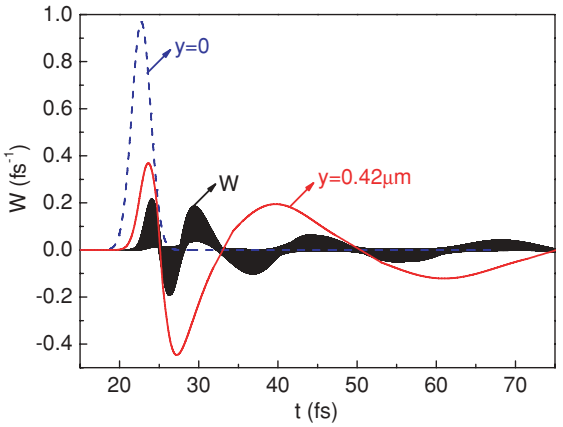

FIG. 3. (Color online) The field work $W(t,y)$ and the envelope $\mathcal{E}(t,y)$ at $y = 0.42$ μm (two-level approximation). Here $\theta = \pi$, $\tau = 2$ fs, $\omega = \omega_{10}$, and $\Gamma = 0$. The envelope $\mathcal{E}(t,0)$ of the input pulse is shown by the dashed line. $\mathcal{E}_0 = 9.69 \times 10^8$ V/cm, $I_0 = 1.25 \times 10^{15}$ W/cm^2.

(FDTD) method with the steps of integration $\delta t = 2\pi/120\omega$ and $\delta y = 2c\delta t$ [8,9]. To reduce the computational costs the simulations are performed for a high concentration of Ar atoms $N = 2.23 \times 10^{21}$ cm^{-3}. Results of the simulations can be easily transformed into the region of lower concentrations N' using the scaling of the propagation distance

$$y' = y\frac{N}{N'}. \tag{14}$$

III. DISCUSSION

A. Field work and stimulated emission

Let us analyze qualitatively here the role of the stimulated emission W_E, which characterizes the competition between Auger decay and stimulated emission. First, we consider the optically thin medium, where the reshaping of the pulse caused by propagation is absent. Figure 2 and Eq. (6) shows that the pulse with the area $\pi \leqslant \theta \leqslant 3\pi$ has one region where the stimulated emission occurs, $W < 0$. Here and in the following the shortened notation $\theta \equiv \theta(\infty)$ is used. According to Eq. (10), the relative Auger yield can be suppressed by such an x-ray pulse.

The role of pulse reshaping during propagation can be well illustrated with a π pulse. The first impression, based on the area theorem [21], is that the stimulated emission is absent for pulses with the area $\theta \leqslant \pi$ and hence the relative Auger

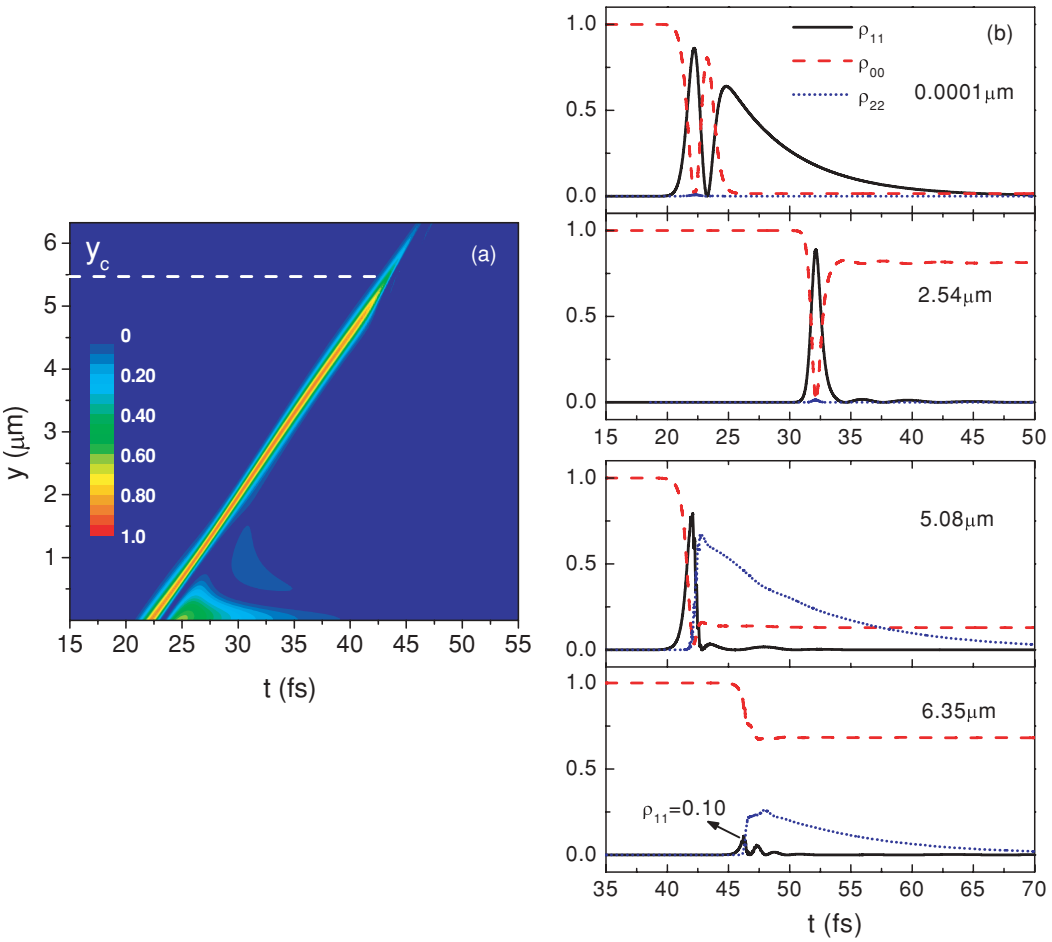

FIG. 4. (Color online) Here $\tau = 2$ fs and $\theta = 3\pi$. (a) The 2-D map of the population of the core-excited state $\rho_{11}(t,y)$. (b) The populations of the ground, core-excited, and final states at different propagation distances $y = 0.0001$, 2.54, 5.08, and 6.35 μm. $\mathcal{E}_0 = 2.91 \times 10^9$ V/cm, $I_0 = 1.12 \times 10^{16}$ W/cm^2.

yield is unchanged $w = 1$. However, the area theorem, derived for an inhomogeneously broadened medium, is valid for the whole pulse area $\theta(\infty, y)$. We need $\theta(t, y)$ and $G(t, y) = \dot{\theta}(t, y)$ to get the instantaneous value of the field work $W(t, y)$ (6). The pulse area $\theta(t, y)$ for a two-level system with $\Gamma = 0$ and without inhomogeneous broadening follows the sine-Gordon equation [22] instead of the McCall-Hahn equation [21]. Due to this fact the envelope of the field $\mathcal{E}(t, y)$ [and the Rabi frequency $G(t, y)$] experiences the Burnham-Chiao (BC) oscillations during propagation [9,22] (see Fig. 3). This results in a sign-changing time dependence of the field work (Fig. 3) for $y > 0$ because $W(t, y)$ is the product of the Rabi frequency $G(t, y)$ and $\sin\theta(t, y)$ (6). Thus the reshaping of the pulse during propagation results in a sign-changing ringing of $W(t, y)$ already for a π pulse. The relative Auger yield $w(y)$ is also already reduced for a π pulse because of the "bursts" of stimulated emission, $W_E \neq 0$ (Fig. 3).

B. Population of the core-excited state and inversion

The population of the core-excited state is another important quantity which characterizes the Auger yield $\rho_{\mathrm{Aug}}(y)$ (5). To give insight in the dependence of the Auger yield and the relative Auger yield on the propagation distance y, let us analyze $\rho_{11}(t, y)$ for a 2 fs pulse. Two-dimensional (2-D) maps of the population of the core-excited state (Figs. 4 and 5) show a rather general trend that the pulse inverts the medium until a critical propagation distance y_c, which is longer for a larger area of the input pulse. The physical meaning of y_c is as follows: The population inversion is quenched for longer propagation distances $y > y_c$ because of the destructive interference of the pump and Stokes fields [9]. The population inversions ρ_{11}-ρ_{00} and ρ_{11}-ρ_{22} created by the pump pulse open the two ASE channels 1-0 and 1-2 with different frequencies ω_{10} and ω_{12}. The beating of the pump field with the Stokes radiation results in a fast sign-changing modulation of the field work $W(t, y)$ with a period of $2\pi/(\omega_{10} - \omega_{12}) \approx 0.17$ fs. This prevents a substantial population of the core-excited state

$$\rho_{11}(t, y) = \int_{-\infty}^{t} e^{-\Gamma(t-t_1)} W(t_1, y) dt_1, \qquad (15)$$

and quenches abruptly the population inversions near the critical propagation distance y_c, where the strength of the two ASE fields becomes comparable. After the critical propagation distance y_c, the ASE channels are blocked and the pulse propagation is affected mainly by the LWI process.

More detailed dynamics of the populations of the ground, core-excited, and final states are shown in Fig. 4(b). It should be pointed out that the quenching of ρ_{11} after $y_c \simeq 5.5\ \mu$m is strong, but it does not mean that $\rho_{11} = 0$. In fact it remains around $\rho_{11} = 0.10$ at $y = 6.35\ \mu$m. Such a 10% population would be very large for conventional synchrotron radiation light sources. This means that the Auger yield which corresponds to $\rho_{11} = 0.10$ is strong enough to be detected. By a comparison of Figs. 4 and 5 one can see that the quenching of ρ_{11} is different for π, 2π, and 3π pulses. Due to this fact the y dependencies of the relative Auger yield for these pulses are also different.

C. Auger yield and relative Auger yield

The Auger yield and relative Auger yield are collected in Figs. 6, 7, and 8 for π, 2π, and 3π pulses with different durations $\tau = 0.25$, 2, 4, and 6 fs. Figure 6 shows a complete breakdown of the two-level approximation ($d_{12} = 0$). The main reason for this is that the ASE in the region $y < y_c$ is followed at $y > y_c$ by lasing without inversion which forms the Stokes band near ω_{12}. The physical reason for the failure of the two-level model is seen directly from the dynamics of the population of the core-excited state [Fig. 4(a)]. This figure displays abrupt quenching of the population of the core-excited state at the critical propagation distance y_c. This quenching caused by the destructive interference of the pump and Stokes fields is absent in two-level atoms which do not create the Stokes radiation. The Stokes radiation enhanced during propagation affects strongly the Auger yield and the

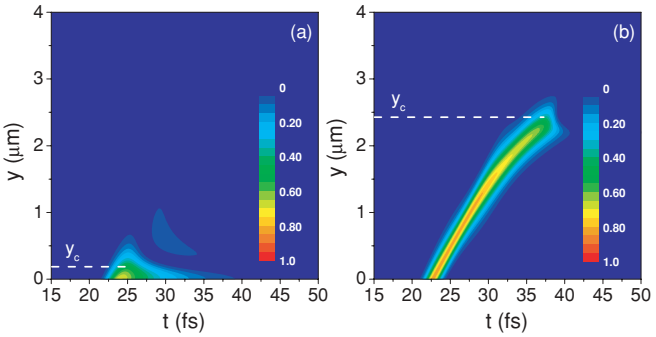

FIG. 5. (Color online) The 2-D map of the population of the core-excited state $\rho_{11}(t, y)$. $\tau = 2$ fs. (a) $\theta = \pi$, $\mathcal{E}_0 = 9.69 \times 10^8$ V/cm, $I_0 = 1.25 \times 10^{15}$ W/cm^2. (b) $\theta = 2\pi$, $\mathcal{E}_0 = 1.94 \times 10^9$ V/cm, $I_0 = 4.98 \times 10^{15}$ W/cm^2.

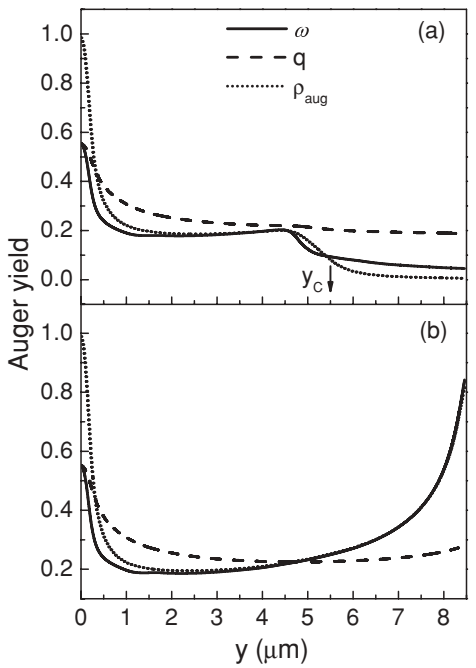

FIG. 6. Comparison of the Auger yield and relative Auger yield for (a) three-level and (b) two-level models. $\tau = 2$ fs. $\theta = 3\pi$ ($I_0 = 1.12 \times 10^{16}$ W/cm^2).

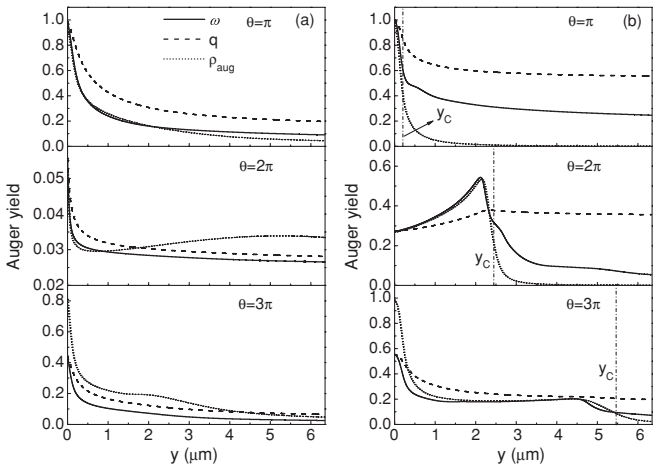

FIG. 7. The Auger yield $\rho_{\mathrm{Aug}}(y)$ (5), relative Auger yield $w(y)$ (10), and the integral relative Auger yield $q(L)$ (12) versus propagation distance for $\theta = \pi$, 2π, and 3π. (a) $\tau = 0.25$ fs, $\theta = \pi$ ($I_0 = 7.98 \times 10^{16}$ W/cm^2), $\theta = 2\pi$ ($I_0 = 3.18 \times 10^{17}$ W/cm^2), $\theta = 3\pi$ ($I_0 = 7.16 \times 10^{17}$ W/cm^2). (b) $\tau = 2$ fs. $\theta = \pi$ ($I_0 = 1.25 \times 10^{15}$ W/cm^2), $\theta = 2\pi$ ($I_0 = 4.98 \times 10^{15}$ W/cm^2), $\theta = 3\pi$ ($I_0 = 1.12 \times 10^{16}$ W/cm^2).

relative Auger yield. As shown in Fig. 6(a), the relative Auger yield w is strongly affected by the Stokes x-ray field after the critical propagation distance y_c. The strong interference between the pump field and the Stokes field quenches the population inversions and suppresses the Auger decay at $y > y_c$ where such a kind of suppression is absent for the two-level system [Fig. 6(b)].

One can see a general trend from Figs. 7 and 8 that the effect of the suppression of the Auger yield and relative Auger yield decreases when the pulse duration increases, especially when it is longer than the lifetime of the core-excited state $\tau > 1/\Gamma = 5.5$ fs. The strongest suppression of the relative

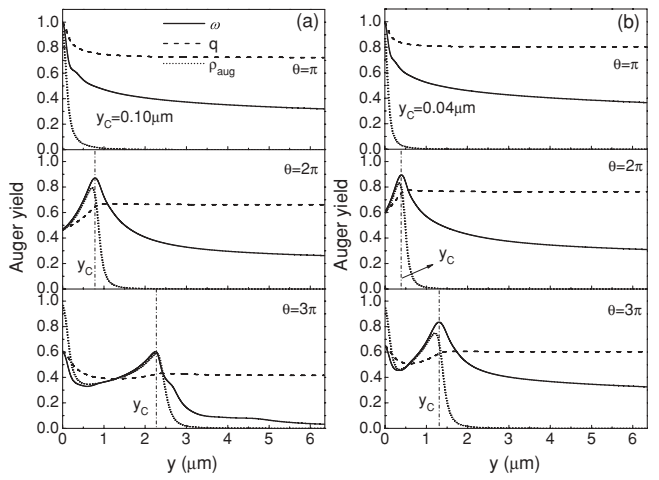

FIG. 8. The Auger yield ρ_{Aug}(y) (5), the relative Auger yield $w(y)$ (10), and the integral relative Auger yield q(L) (12) versus propagation distance for the pulse area $\theta = \pi$, 2π, and 3π. (a) $\tau = 4$ fs, $\theta = \pi$ ($I_0 = 3.11 \times 10^{14}$ W/cm^2), $\theta = 2\pi$ ($I_0 = 1.24 \times 10^{15}$ W/cm^2), $\theta = 3\pi$ ($I_0 = 2.80 \times 10^{15}$ W/cm^2). (b) $\tau = 6$ fs. $\theta = \pi$ ($I_0 = 1.38 \times 10^{14}$ W/cm^2), $\theta = 2\pi$ ($I_0 = 5.51 \times 10^{14}$ W/cm^2), $\theta = 3\pi$ ($I_0 = 1.25 \times 10^{15}$ W/cm^2).

Auger yield (up to $w \lesssim 0.03$) occurs for the shortest 2π pulse with $\tau = 0.25$ fs. The branching ratio for the π pulse starts from ($w = 1$) at $y = 0$ and decreases monotonously during propagation. The reason for this, explained earlier, is the sign-changing modulation of the field work $W(t, y)$, which results in the suppression of the population of the core-excited state. The change of the integral relative Auger yield $q(y)$ along the medium is not so strong in comparison with $w(y)$ since $q(y)$ gives the relative Auger yield collected from the entry up to y.

The evolution of $\rho_{\mathrm{Aug}}(y)$ and $w(y)$ during propagation is rather similar for $\tau = 2, 4$, and 6 fs (Figs. 7 and 8). For example the increase of the relative Auger yield w for the 2π pulses at the beginning is followed by its decrease after the critical propagation distance y_c where w takes maximum. In contrast, the decrease of the relative Auger yield for the 3π pulses at the beginning is followed by the increase of $w(y)$ then the branching ratio decreases after the maximum at $y = y_c$.

To conclude one can say that the Auger yield $\rho_{\mathrm{Aug}}(y)$ and the relative Auger yield $w(y)$ behave similarly in the region where the core-excited state has rather high population $y < y_c$. The $\rho_{\mathrm{Aug}}(y)$ drops down very fast in the region $y > y_c$ where the population of the core-excited state is small. In this region the relative Auger yield is a more appropriate quantity, which shows more accurately the competition between the Auger decay and stimulated emission.

D. Effect of direct photoionization

The main channels of ionization of the studied system are formed by the Auger decay transitions of the core-excited and final states with the relaxation rates Γ and Γ_f. But the strong x-ray radiation can also directly ionize the Ar atoms. Because the photon frequency is below the ionization threshold of the $2p_{3/2}$ electrons, the only ionization channels are the direct ionization of electrons from the outer $3s$ and $3p$ shells. According to the experimental data [14] the corresponding photoionization cross section is about $\sigma_{\mathrm{ph}} \approx 0.3$ Mb. The direct photoionization affects the density matrix equations due to additional relaxations of the populations and of the off-diagonal elements of the density matrix

$$\Gamma_n \to \Gamma_n + \gamma_{\mathrm{ph}}^{(n)}(t), \quad \gamma_{mn} \to \gamma_{mn} + \tfrac{1}{2}\left[\gamma_{\mathrm{ph}}^{(n)}(t) + \gamma_{\mathrm{ph}}^{(m)}(t)\right], \tag{16}$$

caused by the rate of the direct photoionization of the nth level $\gamma_{\mathrm{ph}}^{(n)}(t) = \sigma_{\mathrm{ph}}^{(n)} I(t)/\hbar\omega$, where $I(t) = |E(t)H(t)|$ is the instantaneous intensity of the light. Here we assume $\sigma_{\mathrm{ph}} \approx \sigma_{\mathrm{ph}}^{(0)} \approx \sigma_{\mathrm{ph}}^{(1)} \approx \sigma_{\mathrm{ph}}^{(2)}$, which is a reasonable approximation because the main ionization channel is the ionization of the $3p$ electrons. Figure 9 shows the relative Auger yield with and without direct photoionization for a 2.0 fs pulse with a 3π pulse area. One can see from Fig. 9 that the role of the direct photoionization is not significant for the pulse with an intensity level of 10^{16} W/cm^2. It increases slightly the Auger ratios and does not change very much the dynamics of Auger decay. The main reason for this is the rather long photoionization time $\tau_{\mathrm{ph}} = 1/\gamma_{\mathrm{ph}}^{\max} \approx 11.7$ fs in comparison with the time of Auger decay $1/\Gamma \approx 5.5$ fs and the pulse duration $\tau = 2$ fs.

The core excitation is accompanied also by two-electron transitions which are usually weaker and can be seen in the

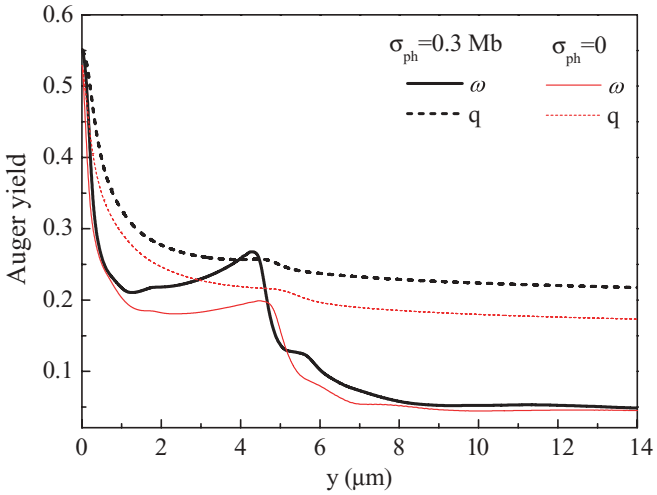

FIG. 9. (Color online) Comparison of relative Auger yield $w(y)$ (10) and $q(L)$ (12) with and without direct photoionization; $\tau = 2$ fs, $\theta = 3\pi$, $I_0 = 1.12 \times 10^{16}$ W/cm^2.

spectrum as weak satellite lines [23,24]. Therefore these weak multi-electron excitations with distinct excitation energies are ignored in our simulations. The second reason for this is that we study resonant scattering where the photon energy is tuned in strict resonance with the one-electron transition. It is also hard to expect that the Stokes and four-wave mixing fields generated in the course of pulse propagation [9] are accidently in resonance with the many-electron transitions.

IV. SUMMARY

We studied the role of propagation of strong x-ray pulses on the resonant Auger effect of atomic Ar at the $2p_{3/2} \rightarrow 4s$ transition. The simulations are performed in a three-level approximation, which includes two radiative decay channels $4s \rightarrow 2p_{3/2}$ and $3s \rightarrow 2p_{3/2}$. The inclusion of the third level is important because it causes drastic reshaping of the spectrum. The pulse power is transferred to the Stokes component $3s \rightarrow 2p_{3/2}$ by stimulated resonant Raman scattering during propagation. The two-level model fails completely due to the propagation effects. We analyze both the Auger yield and the relative Auger yield which show nonmonotonous dependence on the propagation distance. The sign-changing modulation of the field work caused by Burnham-Chiao oscillations results in a quasiperiodical following of the absorption by stimulated emission. This reduces the population of the core-excited state as well as the Auger yield and relative Auger yield. The competition between the Auger decay and the stimulated emission is the main reason for the suppression of the relative Auger yield. In the region where the strength of the pump and Stokes fields becomes comparable, the fast beating oscillation formed by these two fields abruptly quenches the population inversions and strongly suppresses the relative Auger yield. After that, the Stokes lasing occurs without population inversion and the relative Auger yield changes smoothly and slowly due to the small population of the core-excited state.

ACKNOWLEDGMENTS

We acknowledge support from the Swedish Research Council (VR), Carl Tryggers Stiftelse (CTS) foundation, National Natural Science Foundation of China (Grant No. 10974121), and the National Basic Research Program of China (Grant No. 2006CB806000).

[1] C. Bressler and M. Chergui, Chem. Rev. **104**, 1781 (2004).
[2] T. Tschentcher, Chem. Phys. **299**, 271 (2004).
[3] C. Buth, R. Santra, and L. Young, Phys. Rev. Lett. **98**, 253001 (2007).
[4] N. Rohringer and R. Santra, Phys. Rev. A **77**, 053404 (2008).
[5] I. V. Schweigert and S. Mukamel, Phys. Rev. A **78**, 052509 (2008).
[6] D. M. Healion, I. V. Schweigert, and S. Mukamel, J. Phys. Chem. A **112**, 11449 (2008).
[7] Y.-P. Sun, J.-C. Liu, and F. Gel'mukhanov, Europhys. Lett. **87**, 64002 (2009).
[8] Y.-P. Sun, J.-C. Liu, and F. Gel'mukhanov, J. Phys. B: At. Mol. Opt. Phys. **42**, 201001 (2009).
[9] Y.-P. Sun, J.-C. Liu, C.-K. Wang, and F. Gel'mukhanov, Phys. Rev. A **81**, 013812 (2010).
[10] F. Gel'mukhanov and H. Ågren, Phys. Rep. **312**, 87 (1999).
[11] S. P. Hau-Riege, R. A. London, and A. Szoke, Phys. Rev. E **69**, 051906 (2004).
[12] A. Nilsson, O. Björneholm, B. Hernnäs, A. Sandell, and N. Mårtensson, Surf. Sci. **293**, L835 (1993).
[13] K. Siegbahn, C. Nordling, G. Johansson, J. Hedman, P. F. Heden, K. Hamrin, U. Gelius, T. Bergmark, L. O. Werme, and Y. Baer, *ESCA Applied to Free Molecules* (North-Holland, Amsterdam, 1969).
[14] R. Haensel, G. Keitel, N. Kosuch, U. Nielsen, and P. Schreiber, J. Phys. (Paris) **32**, C4-236 (1971).
[15] M. Nakamura, M. Sasanuma, S. Sato, M. Watanabe, H. Yamashita, Y. Iguchi, A. Ejiri, S. Nakai, S. Yamaguchi, T. Sagawa, Y. Nakai, and T. Oshio, Phys. Rev. Lett. **21**, 1303 (1968).
[16] Dalton, References in http://www.kjemi.uio.no/software/dalton/.
[17] J. Nordgren, H. Ågren, C. Nordling, and K. Siegbahn, Phys. Scr. **19**, 5 (1979).
[18] J. Nordgren, H. Ågren, L. Selander, C. Nordling, and K. Siegbahn, Phys. Scr. **16**, 70 (1977).
[19] D. A. Shaw, G. C. King, F. H. Read, and D. Cvejanovic, J. Phys. B **15**, 1785 (1982).
[20] S. L. Sorensen, T. Åberg, J. Tulkki, E. Rachlew-Källne, G. Sundström, and M. Kirm, Phys. Rev. A **50**, 1218 (1994).
[21] S. L. McCall and E. L. Hahn, Phys. Rev. **183**, 457 (1969).
[22] D. C. Burnham and R. Y. Chiao, Phys. Rev. **188**, 667 (1969).
[23] R. Arneberg, H. Ågren, J. Müller, and R. Manne, Chem. Phys. Lett. **91**, 362 (1982).
[24] H. Ågren and R. Arneberg, Phys. Scr. **30**, 55 (1984).